Proteome of Skeletal Muscle Lipid Droplet Reveals Association with Mitochondria and Apolipoprotein A-I

ARTICLE *in* JOURNAL OF PROTEOME RESEARCH · AUGUST 2011

Impact Factor: 4.25 · DOI: 10.1021/pr200553c · Source: PubMed

Journal of proteome research

ARTICLE

pubs.acs.org/jpr

Proteome of Skeletal Muscle Lipid Droplet Reveals Association with Mitochondria and Apolipoprotein A-I

Huina Zhang,[†,‡] Yang Wang,[†,‡,§] Jing Li,[†,‡,§] Jinhai Yu,[†,§] Jing Pu,[†,§] Linghai Li,[†] Hongchao Zhang,[∥] Shuyan Zhang,[†] Gong Peng,[†,§] Fuquan Yang,[*,†] and Pingsheng Liu[*,†]

[†]National Laboratory of Biomacromolecules, Institute of Biophysics, Chinese Academy of Sciences, Beijing, 100101, China

[§]Graduate University of Chinese Academy of Sciences, Beijing, 100049, China

[∥]Department of Cardiac Surgery, Airforce Genral Hospital, Beijing, 100142, China

Supporting Information

ABSTRACT: The lipid droplet (LD) is a universal organelle governing the storage and turnover of neutral lipids. Mounting evidence indicates that elevated intramuscular triglyceride (IMTG) in skeletal muscle LDs is closely associated with insulin resistance and Type 2 Diabetes Mellitus (T2DM). Therefore, the identification of the skeletal muscle LD proteome will provide some clues to dissect the mechanism connecting IMTG with T2DM. In the present work, we identified 324 LD-associated proteins in mouse skeletal muscle LDs through mass spectrometry analysis. Besides lipid metabolism and membrane traffic proteins, a remarkable number of mitochondrial proteins were observed in the skeletal muscle LD proteome. Furthermore, imaging by fluorescence microscopy and transmission electronic microscopy (TEM) directly demonstrated that mitochondria closely adhere to LDs *in vivo*. Moreover, our results revealed for the first time that apolipoprotein A-I (apo A-I), the principal apolipoprotein of high density lipoprotein (HDL) particles, was also localized on skeletal muscle LDs. Further studies verified that apo A-I was expressed endogenously by skeletal muscle cells. In conclusion, we report the protein composition and characterization of skeletal muscle LDs and describe a novel LD-associated protein, apo A-I.

KEYWORDS: lipid droplet, skeletal muscle, mitochondria, apolipoprotein A-I

INTRODUCTION

Neutral lipids are contained in two structures in the body, the cytoplasmic lipid droplet (LD) and lipoproteins carried in the bloodstream.[1] Although these two structures differ with respect to their size, function and location, both lipoprotein particles and LDs have similar forms and may even have the same origin from the endoplasmic reticulum (ER).[2−4] Moreover, traditional lipoprotein specific proteins, the apolipoprotein family members apo B and apo A-V, were recently found associated with lipid droplets (LDs).[5,6] The physiologic roles of lipoprotein particles have been studied for almost 40 years,[7,8] while their intracellular counterparts, lipid droplets, have received close attention only recently.[9]

LDs are an ubiquitous cytoplasmic structure found in the cells of organisms from bacteria to mammals.[1] They are composed of a hydrophobic neutral lipid core surrounded by a protein-coated phospholipid monolayer.[1,10] Much in contrast to their simple structure, LDs have been proposed to have multiple functions,[11] such as lipid metabolism,[12−16] signal transduction,[17,18] protein storage[19] and lipid trafficking.[20] More than 16 proteomic studies have shown that a variety of proteins are either embedded in or associated with LDs, facilitating the multiple functions of this organelle. In addition, based on the characteristics of the identified LD proteins, LDs are suspected to interact with various other cellular compartments including the cytoskeleton,[21] ER,[22,23] endosomes,[24] mitochondria[25] and peroxisomes.[26] However, these studies have been conducted in different species and tissues, precluding a comprehensive view of the LD protein composition.

In humans, LDs are most prominent in adipose cells and steroidogenic cells, but also exist in other cell types. An important but so far unstudied tissue in terms of LD protein composition and LD function is skeletal muscle. Skeletal muscle is the main tissue responsible for insulin-induced glucose disposal in the human body. Furthermore, insulin resistance of skeletal muscle is fundamental to the development of obesity and Type 2 Diabetes Mellitus (T2DM). Accumulated evidence indicates that aberration of intramuscular triglyceride (IMTG) storage in skeletal muscle LDs is more closely linked with insulin resistance and T2DM than excessive storage of lipid in liver and adipose tissue.[27−30] Accordingly, it is important to study the skeletal muscle LD proteome to provide clues to the mechanism linking IMTG and T2DM.

In this study, we carried out proteomic analyses to identify the proteins of LDs purified from skeletal muscle as well as oleic acid-treated C2C12 myotubes. We found 324 proteins in skeletal muscle LDs and almost 72% of them are also identified in LDs of C2C12 myotubes. Among these proteins, 20% (65 proteins) were associated with mitochondria and, among them, 57 proteins were involved in TCA cycle, suggesting close proximity between

Received: June 9, 2011
Published: August 29, 2011

LDs and mitochondria in skeletal muscle. Further studies using fluorescence microscopy and transmission electronic microscopy (TEM) directly demonstrated the interaction of these two organelles *in vivo*. Additionally, a series of high density lipoprotein (HDL)-associated apolipoproteins were identified in the skeletal muscle LD proteome. Immunofluorescence and immunoblotting results confirmed that apo A-I, the main apolipoprotein of HDL, was indeed localized on skeletal muscle LDs. RT-PCR results indicated that apo A-I was expressed by skeletal muscle. Our findings provide some useful information for future studies about the functions of skeletal muscle LDs and give some novel clues to promote the development of T2DM therapeutic treatments.

MATERIALS AND METHODS

Materials

The Colloidal Blue Stain Kit, MitoTracker Green FM and LipidTOX Deep Red were from Invitrogen. The Silver Stain Kit was from Bio-Rad. Oleate and Nile Red was obtained from Sigma-Aldrich. Primary antibody of PDI was from BD. Primary antibodies against Tim23, GAPDH, β-actin, annexin A2, Cav-1, Cav-3, Lamp-1 and EEA1 were purchased from Millipore. Anti-COX IV and anti-BIP were purchased from Cell Signaling Technology. Anti-p62 polyclonal antibody was a gift from Dr. Dorothy Mundy. ADRP monoclonal antibody was a kind gift from Dr. Ginette Serrero. Apo A-I and apo E polyclonal antibody were provided by Dr. H. Hobbs. Acetonitrile and formic acid (FA) were obtained from J. T. Baker.

Culture, Differentiation and Treatment of C2C12 Myoblasts

The C2C12 myoblasts were purchased from American Type Culture Collection and were cultured in DMEM containing 10% FBS, 100 U/mL penicillin and 100 μg/mL streptomycin. When in 90% confluent, myoblasts were transferred to differentiation medium consisting of DMEM with 2% horse serum and antibiotics and differentiated for 7 days. C2C12 myotubes were treated with oleate (200 μM) for 12 h before experiments.

LD Purification

All of the animal protocols were approved by the Animal Care and Use Committee at the Institute of Biophysics Chinese Academy of Sciences under the permission number SCXK (SPF2009−111). LDs were purified by a modified method of Liu et al.[31] Briefly, we collected skeletal muscle (from hind legs of twenty C57B/L6 mice) or livers (from two C57B/L6 mice) or 10^9 cells from cultured, oleate-incubated C2C12 myotubes and put them into ice-cold PBS containing 0.2 mM PMSF. For skeletal muscle and liver, fascia and other connective tissues were carefully removed. Then all the tissues were transferred to 12 mL buffer A (25 mM tricine pH 7.6, 250 mM sucrose) plus 0.2 mM PMSF, homogenized with a Dounce type glass-Teflon homogenizer on ice (20 times for skeletal muscle, and 10 times for liver). For C2C12 myotubes, after centrifugation at 1000× *g*, pellets were resuspended in 12 mL buffer A plus 0.2 mM PMSF, homogenized with a Dounce type glass-Teflon homogenizer on ice for 10 times. All the homogenate from tissues and cells were centrifuged at 100× *g* to remove the debris and the cell suspension was further homogenized by N_2 bomb (500 psi for 15 min on ice). The postnuclear supernatant (PNS) fraction (10 mL) with 2 mL buffer B (20 mM HEPES, pH 7.4, 100 mM KCl, and 2 mM $MgCl_2$) was obtained by centrifugation at 3000× *g* and loaded into a SW40 tube. The sample was centrifuged at 300 000× *g* for 1 h at 4 °C. The white band containing lipid droplets at the top of gradient was collected in 0.5 mL, then the sample was centrifuged at 20 000× *g* for 3 min, the underlying solution was carefully removed, and droplets were gently resuspended in 200 μL of buffer B. This procedure was repeated four times until all underlying solution was removed, then the sample was ready for biochemical, morphological, and functional analysis. For detailed protocol of "Isolation of skeletal muscle lipid droplets", please see Supporting Information 1 (SI1).

Transmission Electron Microscopy

Mouse skeletal muscle tissue and isolated lipid droplets were examined by transmission electron microscopy (TEM) using ultrathin sectioning and negative staining respectively. The skeletal muscle tissue was prefixed in 2.5% (w/v) glutaraldehyde in PBS (pH 7.4) for 2 days at 4 °C and postfixed in 2% (w/v) osmium tetraoxide for 1 h at 4 °C. Dehydration was carried out in an ascending concentration series of ethanol at room temperature. Then samples were embedded in Quetol 812 and sectioned to a thickness of 90 nm with Leica EM UC6 Ultramicrotome (Leica Company). The section was stained with 2% (w/v) uranyl acetate for 15 min and with lead citrate for 5 min at room temperature. Then the stained section was viewed with a FEI Tecnai20 (FEI company) electron microscope. The isolated lipid droplets were placed on a Formvar-carbon coated copper grid and stained for 30 s by adding an equal volume of 2% (w/v) uranyl acetate. Then the grid was viewed with a FEI Tecnai 20 electron microscope.

Protein Preparation and Immunoblotting

LD proteins were precipitated by 100% acetone at room temperature, dissolved in SDS sample buffer and denatured at 95 °C for 5 min followed by a brief centrifugation at 10 000× *g*. Cells were lysed directly with 2 × SDS loading buffer, sonicated and denatured at 95 °C for 5 min. Mouse tissue samples were prepared according to a previously published method.[32] Briefly, wet tissues were dissolved in 2 × SDS loading buffer by sonication. After 10-fold dilution with PBS, the protein samples were precipitated in 7.2% trichloroacetic acid (TCA), and then washed with acetone before dissolving in 2 × SDS loading buffer by sonication. Total proteins were fractionated by 10% SDS−PAGE then either stained with a silver stain kit essentially as previously reported[33] or transferred to a PVDF membrane for immunoblotting. Immunoblotting was performed with the antibodies indicated and detected by ECL system as described previously.[31] Colloidal Blue Staining was used as loading control.

Fluorescence Microscopy in C2C12 Myoblasts

C2C12 myoblasts were incubated with Nile Red (0.05 μg/mL) for 10 min at 37 °C. For mitochondrion and lipid droplet staining, 25 nM MitoTracker Green FM and 1:1000 diluted LipidTOX Deep Red were prepared in complete medium and incubated C2C12 myoblasts for 30 min at 37 °C. Fluorescence images were obtained by Olympus FV500 confocal microscope.

Immunofluorescence

The rabbit antiapo A-I and apo E polyclonal antibodies and anti-PDI monoclonal antibody were used for the immunofluorescence experiments. Briefly, cells were fixed with 4% paraformaldehyde and pretreated with 0.2% Triton X-100 in phosphate-buffered saline (PBS) for 15 min. After blocking with 2% goat serum, the cells were incubated sequentially with primary antibody and fluorescence-conjugated secondary antibody at room temperature for 1 h each. The cells were then stained with

LipidTOX Deep Red and/or Hoechst 33258 and images were captured with an Olympus FV500 fluorescence microscope.

Human Tissue Collection

The study design was approved by the Medical Ethical Committee of Airforce General Hospital (AGH). Informed consent was obtained from tissue donors' parents. The research protocols were approved by the Board of Ethics at AGH. The total tissue samples were harvested from a patient who received primary corrective cardiac surgery for Tetralogy of Fallot (TOF). The patient was an 18 years female and a body weight of 56.6 kg. Diagnoses of TOF was obtained by chest X-ray, electrocardiography, echocardiography and confirmed by surgical observation. When right ventricular outflow tract obstruction was reconstructed, the tissues were collected according to procedure. The skeletal muscle sample was taken from pectoral muscle and the heart sample from muscular trabeculae of the endocardial surface of the right ventricular outflow tract. All the samples were stored in liquid nitrogen for RT-PCR assay.

RT-PCR

Total RNA was extracted using TRIzol reagent (Invitrogen) according to the manufacture's protocol. Two micrograms of total RNA were used to synthesize first-strand with cDNA with M-MuLV reverse transcriptase (New England Biolabs) using random primers. Semiquantitative reverse transcription PCR (RT−PCR) was used to analyze apo A-I mRNA level in skeletal muscle. Primers used in PCR were:

gene		sequences (5′ → 3′)	Amplicon
mouse apo A-I_1	for	GGATTTCGCTAATGTGTATG-TGGATG	**566bp**
	rev	GTGTCTTCAGGTGGGTTTTGGC	
mouse apo A-I_2	for	TGACTCGGGACTTCTGGGATAA	**401bp**
	rev	TGTCTTCAGGTGGGTTTTGGC	
mouse apo B100	for	ATCAGAGAAGGGTCAAAGAATG	**499bp**
	rev	TGGAGTAAGCTCCTGTGGTAC	
mouse apo E	for	TCTGGTGGAGCAAGGTCGC	**340bp**
	rev	CACTGGGGTGATGATGGGG	
mouse GAPDH	for	GGAAACTGTGGCGTGATGG	**413bp**
	rev	GTAGGCCATGAGGTCCACCA	
human apo A-I	for	TCAAAGACAGCGGCAGAGA	**269bp**
	rev	GGAAGTCGTCCAGGTAGGG	
human and mouse β-actin	for	GGCACCACACCTTCTACAATGAG	**386bp**
	rev	CTTTGATGTCACGCACGATTTC	
human GAPDH	for	AACAGCCTCAAGATCATCAGCAA	**468bp**
	rev	AGCGTCAAAGGTGGAGGAGTG.	

In-solution Digestion and 2D-LC−MS/MS Analysis

The LD protein pellet was dissolved in 20 μL of freshly prepared 8 M urea, reduced with 10 mM DTT at 56 °C for 1 h, and treated with 40 mM iodoacetamide in the dark for 45 min to block the sulfhydryl groups. A second addition of DTT to a final concentration of 40 mM was made to quench any remaining iodoacetamide. The sample was then diluted with 25 mM NH_4HCO_3 (pH 8.0) to reduce the concentration of urea to below 1 M. Trypsin was added to a ratio of 1:60 relative to total protein content and the sample was incubated at 37 °C for 12 h. A second, equivalent aliquot of trypsin was added and the sample was incubated in 37 °C for another 6 h before FA was added to end the digestion. The sample was then centrifuged at 14 000× g for 10 min and the supernatant was collected and stored at −20 °C until use.

The tryptic peptide mixtures were analyzed by a 2D-HPLC system coupled to a linear ion trap mass spectrometer LTQ ion trap (Thermo Fisher Scientific, Waltham, MA). For single analysis, the peptide mixtures (from about 30 μg and 50 μg proteins for tissue and cell LDs, respectively) was pressure-loaded onto a biphasic silica capillary column (250 μm id) packed with 3 cm of reverse phase C18 resin (SP-120-3-ODS-A, 3 mm, the Great Eur-Asia Sci & Tech Development, Beijing, China) and 3 cm of strong cation exchange resin (Luma 5 m SCX 100A, Phenomenex, Torrance, CA). The buffers used were 0.1% FA (buffer A), 80% ACN/0.1% FA (buffer B), and 600 mM ammonium acetate/5% ACN/0.1% FA (buffer C). After sample loading, the biphasic column was first desalted with buffer A and then eluted using a 3-step salt gradient ranging from 0 to 600 mM ammonium acetate. Step 1 consisted of a 100-min gradient from 0 to 100% buffer B. For step 2, after equilibrating with buffer A for the first 3 min, 35% buffer C was applied for 5 min, and peptides were eluted using a gradient as follows: 0−10% buffer B in 5 min, 10−45% buffer B in 77 min, 45−100% buffer B in 10 min and 100% buffer B for 10 min, followed by re-equilibration with buffer A for 10 min. The gradient used in the final step contained 3 min of 100% buffer A, 20 min of 100% buffer C, a 5-min gradient from 0 to 10% buffer B, a 72-min gradient from 10 to 55% buffer B and a 5-min gradient from 55 to 100% buffer B. Then 100% buffer B was applied for 5 min, followed by a 5-min elution with buffer A and another 10-min elution with buffer B. The effluent of the biphasic column in each case was directed into an in-house-packed 10 cm C18 analytical column (100 μm id, SP-120−3-ODS-A, 3 μm) with a 3- to 5-μm spray tip, where the flow rate was maintained at about 500 nL/min. Nanoelectrospray ionization was performed at a spray voltage of 2.0 kV and a heated capillary temperature of 160 °C. The MS instrument was set to the data-dependent acquisition mode with dynamic exclusion turned on, and maximum ion injection time was set to 100 ms. One MS survey scan, with mass range 400−2000 m/z, was followed by five MS/MS scans. All tandem mass spectra were collected using normalized collision energy (a setting of 35%), an isolation window of 2 m/z, and 1 microscan. The XCalibur data system (ThermoElectron, Waltham, MA) was used to control the HPLC solvent gradients and the application of MS scanning functions.

MS/MS data were searched using SEQUEST algorithm (Ver. 2.8) against the NCBI Refseq mouse database that was released on Jan. 3, 2011. The database was reversed and attached to estimate the false discovery rate (FDR). All searches were performed using a precursor mass tolerance of 3 Da calculated using average isotopic masses. Fixed modification was set for cysteine with an addition of 57.052 Da to represent cysteine carboxyamidation, and variable modification was set for methionine with an addition of 15.999 Da to represent methionine oxidation. A fragment ion mass tolerance of 1 Da (monoisotopic mass) was used. Enzyme cleavage specificity was set to trypsin and no more than two missed cleavages were allowed. The SEQUEST outputs were then analyzed using the commercial software Thermo Electron BioWorks (Rev.3.3.1). The filter settings for peptides were as follows − XCorr ≥1.5 (+1 ions), 2.0(+2 ions), 2.5(+3 ions); Delta CN ≥ 0.08; Sp ≥ 500; Rsp ≤5. The FDR for every single experiment calculated by dividing the absolute number of reversed hits through the true hits against the

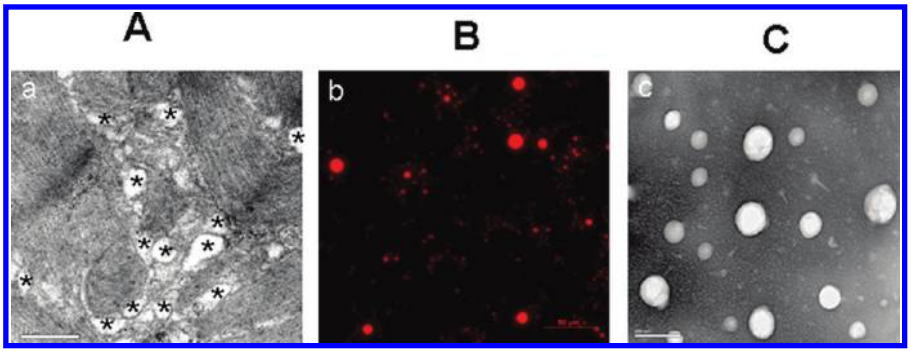

Figure 1. Morphology of mouse skeletal muscle LDs. (A) Mouse skeletal muscle was sectioned to 90 nm thick, stained with 2% uranyl acetate and observed by TEM. Asterisks indicate the sites of LDs. Bar = 0.5 μm. (B) LDs isolated from mouse skeletal muscle were stained with 0.05 μg/mL Nile Red for 15 min and imagined by fluorescence microscope. Bar = 50 μm. (C) LDs isolated from mouse skeletal muscle were stained with 2% (w/v) uranyl acetate for 30 s and observed by TEM. Bar = 200 nm.

actual database was about 1%. At the protein level, obviously contaminant proteins such as keratins were manually deleted and only proteins with at least two different peptides were accepted.

Data Mining and Bioinformatics

To obtain comprehensive and reliable identification results, two biological replicates were carried out and the results were combined for further analysis. Additionally, oleate-treated C2C12 myotubes were also chosen as a homogeneous comparison sample to exclude contaminating proteins from adjacent skeletal muscle structures. The physicochemical characteristics of the identified proteins were analyzed using free online tools: protein molecular weights and IEF points were calculated using ExPASy tools;[34] the calculation of protein GRAVY (grand average of hydropathy) values was performed using Protein GRAVY.[35] The function and subcellular location of all the identified proteins were annotated according to Gene Ontology Annotation (GOA) database descriptions[36] and the proteins were thus manually categorized. Protein associations were revealed by the Web site program String.[37]

RESULTS

Isolation of LDs from Mouse Skeletal Muscle

LDs can be visualized in mouse skeletal muscle using transmission electron microscopy (TEM). As shown in Figure 1A, clusters of LDs were readily visible in skeletal muscle fibers. Intramuscular triglyceride (IMTG) has been correlated with insulin resistance of skeletal muscle. Since LDs in muscle cells have not been explored, we carried out several experiments to study muscle LDs. First, LDs were purified from mouse skeletal muscle tissue by a modified method described previously[31](SI1, Supporting Information). The quality of the preparation was assessed by fluorescence microscopy using Nile Red staining and by electron microscopy using negative staining. As shown in Figure 1B, all LDs stained with Nile Red appeared intact. Aside from few large LDs, most droplets were smaller than 1 μm diameter. To further examine the morphology as well as purity of LD preparations, LDs were negative-stained and observed by electron microscopy. Consistent with the fluorescence images, LDs were found to be intact with a spherical shape and varying in size but were less than 1 μm in diameter. More importantly, LDs were also the predominant structures in the field of view (Figure 1C).

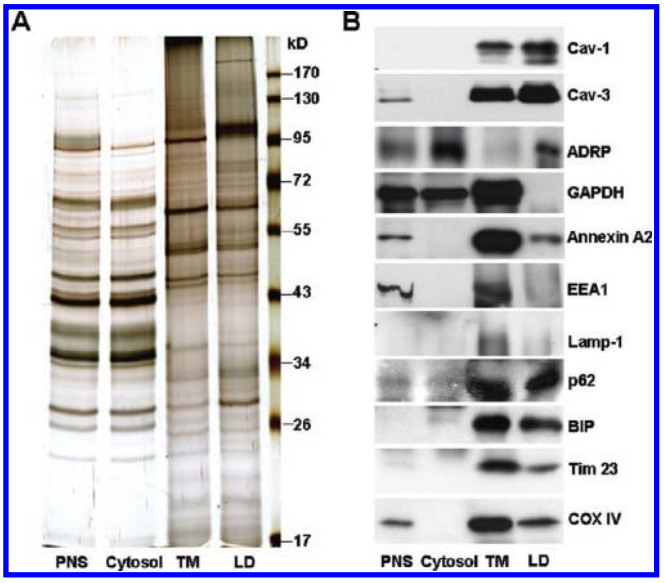

Figure 2. Unique protein pattern of LDs isolated from mouse skeletal muscle. LD proteins from mouse skeletal muscle were dissolved by SDS sample buffer. Twenty micrograms of LD proteins were loaded and separated by 10% SDS-PAGE along with equal amount proteins from postnuclear supernatant (PNS), cytosol and total membrane (TM). (A) Silver Stained Gel was used to compare the protein profiles of different cellular fractions. (B) Proteins separated by SDS-PAGE were transferred to a PVDF membrane, and immunoblotted with indicated antibodies. The primary antibodies of Cav-1, Cav-3 and ADRP were utilized to confirm the enrichment of LDs. GAPDH (cytosol), Annexin A2 (plasma membrane), EEA1 (early endosome), Lamp-1 (lysosome), p62 and BIP (endoplasmic reticulum), Tim 23 and COX IV (mitochondrion) antibodies were utilized individually to detect contamination from other cellular components.

The purity of the isolated LDs was critical for further proteomic study. Therefore, to determine the purity using more stringent criteria, we made biochemical measurement in addition to the morphologic evaluation. First, we compared protein profile of LD to other cell fractions by using Silver-staining. Proteins extracted from LDs displayed a relatively simple pattern that was obviously distinct from the protein profiles of the other three cellular fractions, including postnuclear supernatant (PNS), total membranes (TM) and cytosol (Figure 2A). Besides the unique protein pattern, the purity of isolated LDs was further

assessed by the relative enrichment of LD-resident proteins caveolin-1, muscle specific caveolin-3 and adipose differentiation-related protein (ADRP), and the absence of markers that correspond to other intracellular compartments, early endosome protein EEA1, lysosome protein Lamp-1, and cytoplasmic protein GAPDH. In addition, as previous reported,[38] the cell membrane protein annexin A2 was detected in our LD prep. Two ER proteins, p62 (ER membrane protein) and BIP (ER luminal protein), as well as two mitochondrial membrane proteins (Tim 23 and COX IV), were found in the LD fraction (Figure 2B). Collectively, these results suggest that the isolated LD fraction from skeletal muscle was largely free of contamination except for ER and mitochondria. These results are consistent with previous reports that LDs interact with mitochondria, mediated by SNAP 23,[39] and with ER, mediated by Rab 18.[22,23]

Proteomic Analysis of Skeletal Muscle LDs

The proteins extracted from isolated LDs were digested with trypsin and analyzed by 2D-LC-MS/MS. To enhance the validity of the data, only proteins with at least two unique peptides were accepted. 324 proteins were identified on LDs of skeletal muscle. Among the proteins, 90 have been identified previously (Table 1), indicating the accuracy of the purification and proteomic techniques. We also analyzed LDs isolated from oleate-treated C2C12 myotubes, providing a sample from a homogeneous source for comparison. Roughly 72% of the proteome from the skeletal muscle sample was also found in the LDs from C2C12 myotubes (Figure 3A, Table 1 and SI7, Supporting Information), demonstrating the quality of the preparations. The divergence in the remaining 28% of the identified proteins (91 proteins) was most likely due the different cellular sources (animal tissue versus an immortalized cell line) and the difference in treatment (untreated versus oleate treated). As illustrated in the Venn diagram (Figure 3A) the 233 proteins shared by both preparations are probably most faithfully associated with LDs of muscle cells.

All of the identified proteins (324) were categorized into groups based on their functional characterization or subcellular locations (Table 1 and Figure 3B). As shown in Figure 3B, purified lipid droplets were selectively enriched in mitochondrial proteins (20%, 65 proteins) and most of them (57 of 65) were TCA cycle-related enzymes (Table 1), suggesting the intimate metabolic relationship between LDs and mitochondria in skeletal muscle. Another major group was membrane traffic proteins (representing an equal share compared with the mitochondria group) including Rabs, SNAREs and coatomers (Table 1), many of which have been reported to be associated with LDs before. As previously reported, these proteins were involved in dynamic activities of the LDs including interaction with other organelles,[22,24] fusion[40] and PAT-family protein recruitment.[41] The third notable group of the identified LD-associated proteins included cytoskeleton proteins, constituting approximately 16% of the total (Figure 3A and SI6, Supporting Information). The finding of abundant cytoskeleton proteins on LDs not only supported the contribution of the cytoskeleton during LD transport as previously reported[21] but also raised another possibility that the cytoskeleton in skeletal muscle may maintain LDs in a proper location. Another group was composed of 34 lipid metabolic enzymes (about 10% of the total) involved in metabolism of triglycerides, fatty acids, phospholipids, and sterol esters (Figure 3A and Table 1). This is in agreement with the role of the LD as a neutral lipid storage and metabolic compartment. The most unexpected finding in the proteome was the identification of a series of HDL-associated apolipoprotein members consisting of apo A-I, apo A-II, apo C-III and apo E. Previous studies reported that other apolipoproteins including apo B, apo A-V, apo E and apo O were localized on LDs of hepatocytes and cadiocytes, respectively. The proteins are through to mediate lipid homeostasis or protect cells from lipoapoptosis.[5,6,42] However, the precise function of apolipoproteins on droplets remains unknown.

The web-based program String was employed to analyze the associations among the identified proteins from mouse skeletal muscle LDs and the metabolic proteins, respectively (Figure 3C and SI5, Supporting Information). Among the total 324 identified proteins, 303 had entries in the String database and 1745 associations of different types were depicted by specifically colored lines as shown in Supporting Information 5 (SI5). For the metabolic proteins plus apolipoproteins, the figure depicts 36 proteins and 98 associations (Figure 3C). The protein association networks enabled us to analyze the identified proteins systematically. On one hand, some proteins showed close relationship between each other, forming unique protein clusters. Consistent with our functional classification, the most dense interaction networks contained metabolism and membrane trafficking related proteins. The protein clusters can also lead insights into unknown protein functions. For example, the apolipoproteins were found to have close relationship with the carnitine palmitoyltransferase Cpt1b and Cpt2, suggesting their possible roles in the metabolism of palmitoylcarnitine into palmitoyl-CoA. In addition, the protein association network can also provide valuable clues for protein localization. We are interested in the proteins that showed close interactions with the known LD proteins, as they should also be LD proteins or LD-associated proteins. For the proteins known to be located in other organelles, their interaction with the LD proteins could provide evidence for the association between LDs with those organelles.

Verification of the Interaction between LDs and Mitochondria

Both mass spectrometry identification (Figure 3B) and immunoblotting results (Figure 2B) indicated that mitochondria were tightly associated with LDs in skeletal muscle. To determine the extent to which mitochondria associate with LDs, oleate-treated C2C12 cells were stained with MitoTracker (green, mitochondrial staining) and LipidTOX (red, lipid droplet staining) simultaneously for observation by laser confocal scanning microscopy. As shown in Figure 4A, we found that many large LDs were surrounded by or in direct contact with mitochondria. To examine with more certainty the physical interactions between mitochondria and LDs at higher resolution, ultrathin sections of skeletal muscle tissue were analyzed by TEM. Consistent with the fluorescence microscopy results, contacts between mitochondria and LDs were easily detected in skeletal muscle tissue, giving additional experimental support for the proximity of mitochondria and LDs (Figure 4B).

Apo A-I Was Associated with LDs and Expressed Endogenously by Skeletal Muscle

Apo A-I, the principal apolipoprotein of HDL, has been well studied due to its role in formation of HDL, which provides a cardiovascular protective effect. Our mass spectrometry results indicated that apo A-I was associated with LDs in skeletal muscle (Table 1). To further verify these results, immunoblotting and immunofluorescence imaging were used separately to detect the location of apo A-I. Consistent with proteomic data, apo A-I protein was detected on LDs of skeletal muscle, oleate-treated C2C12 as well as mouse liver (Figure 5A, B and SI2, Supporting

Table 1. Part of Skeletal Muscle Lipid Droplet Proteins Identified by Mass Spectrometry[α]

gene symbol	GI no.	description	reported
		lipid metabolism	
Pla2g4a	6679369	cytosolic phospholipase A2	√
Acsl1	31560705	long-chain-fatty-acid--CoA ligase 1	√
Acsl3	75992920	long-chain-fatty-acid--CoA ligase 3 isoform a	√
Acsl4	46518528	long-chain-fatty-acid--CoA ligase 4 isoform 1	√
Hsd17b7	87162470	3-keto-steroid reductase	√
Lipe	87239970	hormone-sensitive lipase isoform 1 (HSL)	√
Acsl3	209977076	long-chain-fatty-acid--CoA ligase 3 isoform b	√
Dhrs3	289063391	short-chain dehydrogenase/reductase 3 isoform 2	
Nsdhl	31982437	sterol-4-alpha-carboxylate 3-dehydrogenase, decarboxylating	√
Acadl	31982520	long-chain specific acyl-CoA dehydrogenase, mitochondrial precursor	
Agpat6	30520301	glycerol-3-phosphate acyltransferase 6	
Hsd17b11	16716597	estradiol 17-beta-dehydrogenase 11	√
Abhd5	13385690	1-acylglycerol-3-phosphate *O*-acyltransferase ABHD5 (CGI-58)	√
Rdh14	12963791	retinol dehydrogenase 14	
Lss	22122469	lanosterol synthase	√
Acadvl	23956084	very long-chain specific acyl-CoA dehydrogenase, mitochondrial precursor	
Rdh10	25141231	retinol dehydrogenase 10	
Echs1	29789289	enoyl-CoA hydratase, mitochondrial precursor	
Hsdl1	30424792	inactive hydroxysteroid dehydrogenase-like protein 1	
Lpcat4	46402175	lysophospholipid acyltransferase LPCAT4	
Pcyt1b	46877071	choline-phosphate cytidylyltransferase B isoform 1	
Alox5	62526037	arachidonate 5-lipoxygenase	
Hsd3b7	100817048	3 beta-hydroxysteroid dehydrogenase type 7 isoform b	√
Pgs1	110626163	CDP-diacylglycerol--glycerol-3-phosphate 3-phosphatidyltransferase, mitochondrial	
Pcyt1a	253683458	choline-phosphate cytidylyltransferase A	
Pnpla2	254826780	patatin-like phospholipase domain-containing protein 2 isoform 1 (ATGL)	√
Sccpdh	30520019	probable saccharopine dehydrogenase (CGI-49)	√
Hsd17b4	31982273	peroxisomal multifunctional enzyme type 2	√
Mgll	261878509	monoglyceride lipase isoform c	√
Hadha	33859811	trifunctional enzyme subunit alpha, mitochondrial precursor	
Hadhb	21704100	trifunctional enzyme subunit beta, mitochondrial precursor	
Cpt2	162138915	carnitine *O*-palmitoyltransferase 2, mitochondrial precursor	
Cpt1b	162287165	carnitine *O*-palmitoyltransferase 1, muscle isoform	
Pisd	126722757	phosphatidylserine decarboxylase proenzyme	
		Membrane traffic	
Vamp3	6678553	vesicle-associated membrane protein 3	
Sypl2	6678874	synaptophysin-like protein 2	
Sypl	41282044	synaptophysin-like protein 1 isoform 2	
Vat1	33859662	synaptic vesicle membrane protein VAT-1 homologue	√
Irgm1	6680351	immunity-related GTPase family M protein 1	
Dnm1l	71061455	dynamin-1-like protein isoform b	
Opa1	19526960	dynamin-like 120 kDa protein, mitochondrial isoform 2 precursor	
Tmed9	145966911	transmembrane emp24 domain-containing protein 9 precursor	√
Tmem43	21311891	transmembrane protein 43	
Sar1b	21313476	GTP-binding protein SAR1b	
Arl8a	23956194	ADP-ribosylation factor-like protein 8A	
Arl8b	13385518	ADP-ribosylation factor-like protein 8B	√
Cltc	51491845	clathrin heavy chain 1	√
Dysf	116174791	dysferlin isoform 1	
Myof	153791796	myoferlin	
Anxa2	6996913	annexin A2	√
Anxa1	124517663	annexin A1	

Table 1. Continued

gene symbol	GI no.	description	reported
Anxa6	158966670	annexin A6 isoform b	√
Vcp	225543319	transitional endoplasmic reticulum ATPase	√
Vps13a	66392160	vacuolar protein sorting-associated protein 13A	
Vps4a	18699726	vacuolar protein sorting-associated protein 4A	√
Vps13d	189491889	vacuolar protein sorting-associated protein 13D	
Vps13c	122114537	vacuolar protein sorting-associated protein 13C	
Use1	224809387	vesicle transport protein USE1 isoform 3	
Fis1	253735731	mitochondrial fission 1 protein isoform 2	
Bin1	6753050	myc box-dependent-interacting protein 1 isoform 1	
Ehbp1l1	167736349	EH domain-binding protein 1-like protein 1 isoform D	
Ehbp1l1	167736351	EH domain-binding protein 1-like protein 1 isoform a	
Ehd2	55742711	EH domain-containing protein 2	√
Ehd4	31981592	EH domain-containing protein 4	
Arl6ip5	14149750	PRA1 family protein 3	
Scp2	45476581	nonspecific lipid-transfer protein	
Rtn2	70778920	reticulon-2 isoform C	
Snx1	71043944	sorting nexin-1	
Trim72	121247302	tripartite motif-containing protein 72	
Gbas	160298168	protein NipSnap homologue 2	
Rab1	6679587	ras-related protein Rab-1A	√
Rab1b	21313162	ras-related protein Rab-1B	√
Rab2a	10946940	ras-related protein Rab-2A	√
Rab2b	30525051	ras-related protein Rab-2B	√
Rab3a	6679593	ras-related protein Rab-3A	√
Rab4a	171184402	ras-related protein Rab-4A	
Rab4b	21313012	ras-related protein Rab-4B	
Rab5a	13385374	ras-related protein Rab-5A	√
Rab5b	28916687	ras-related protein Rab-5B isoform 1	√
Rab5c	113866024	ras-related protein Rab-5C	√
Rab7	148747526	ras-related protein Rab-7a	√
Rab8a	38372905	ras-related protein Rab-8A	√
Rab8b	27734154	ras-related protein Rab-8B	
Rab10	7710086	ras-related protein Rab-10	√
Rab11a	31980840	ras-related protein Rab-11A	√
Rab11b	6679583	ras-related protein Rab-11B	√
Rab12	106507168	ras-related protein Rab-12	
Rab13	21311975	ras-related protein Rab-13	
Rab14	18390323	ras-related protein Rab-14	√
Rab18	30841008	ras-related protein Rab-18	√
Rab21	33859751	ras-related protein Rab-21	√
Rab22a	148747177	ras-related protein Rab-22A	
Rab24	6679591	ras-related protein Rab-24	√
Rab31	225579124	ras-related protein Rab-31	
Rab34	31560774	ras-related protein Rab-34	√
Rab35	37718983	ras-related protein Rab-35	√
		Cell signal	
Calm1	6753244	calmodulin	
Cdc42	6753364	cell division control protein 42 homologue precursor	
Rhog	9625037	rho-related GTP-binding protein RhoG precursor	√
Ralb	11612509	ras-related protein Ral-B precursor	√
Rac3	18875380	ras-related C3 botulinum toxin substrate 3 precursor	
Cdc42ep1	21312428	cdc42 effector protein 1	
Rap1a	21704066	ras-related protein Rap-1A precursor	√
Rap1b	33859753	ras-related protein Rap-1b precursor	√

dx.doi.org/10.1021/pr200553c |J. Proteome Res. 2011, 10, 4757–4768

Table 1. Continued

gene symbol	GI no.	description	reported
1500003O03Rik	9790225	calcium-binding protein p22	√
Ldb3	84872213	LIM domain-binding protein 3 isoform b	
Ldb3	84872217	LIM domain-binding protein 3 isoform f	
Ptpmt1	23956130	protein-tyrosine phosphatase mitochondrial 1	
Map2k2	31560267	dual specificity mitogen-activated protein kinase kinase 2	
Ryr1	145046267	ryanodine receptor 1, skeletal muscle	
Kras	266458391	GTPase KRas	√
Pdlim5	300069024	PDZ and LIM domain protein 5 isoform ENH1e	
Gnb1	6680045	guanine nucleotide-binding protein G(I)/G(S)/G(T) subunit beta-1	
Gnb2	13937391	guanine nucleotide-binding protein G(I)/G(S)/G(T) subunit beta-2	
Pdlim7	166197681	PDZ and LIM domain protein 7 isoform a	
Casq1	227430322	calsequestrin-1	
Srl	34328417	sarcalumenin precursor	
Faf2	158533976	FAS-associated factor 2	√
Ahnak	61743961	AHNAK nucleoprotein isoform 1	
Obscn	284005473	obscurin isoform 2	
Elmod2	283436077	ELMO domain-containing protein 2	
		Lipid droplet	
Plin3	13385312	perilipin-3 (Tip47)	√
Plin2	116235489	perilipin-2 (Adfp)	√
Plin4	157041252	perilipin-4 (S3−12)	√
		Apolipoprotein	
Apoc3	15421856	apolipoprotein C−III precursor	
Apoa2	157951676	apolipoprotein A-II precursor	
Apoa1	160333304	apolipoprotein A-I preproprotein	
Apoe	163644329	apolipoprotein E precursor	√
		Chaperone	
Hspa8	31981690	heat shock cognate 71 kDa protein	√
Hsp90ab1	40556608	heat shock protein HSP 90-beta	√
Cabc1	70778882	chaperone activity of bc1 complex-like, mitochondrial precursor	
Hspa1l	124339838	heat shock 70 kDa protein 1-like	
Hspa9	162461907	stress-70 protein, mitochondrial	√
Hspd1	183396771	60 kDa heat shock protein, mitochondrial	√
Prdx1	6754976	peroxiredoxin-1	√
Hspa2	31560686	heat shock-related 70 kDa protein 2	
Hsp90b1	6755863	endoplasmin	√
Hspa5	254540166	78 kDa glucose-regulated protein precursor	√
Canx	160333216	calnexin precursor	√
Serpinh1	161353506	serpin H1 precursor	
		Endoplasmic reticulum	
Atp2a2	6806903	sarcoplasmic/endoplasmic reticulum calcium ATPase 2 isoform b	√
Atp2a1	36031132	sarcoplasmic/endoplasmic reticulum calcium ATPase 1	
Hrc	133778931	histidine rich calcium binding protein	

[a] Lipid droplet proteins were extracted from mouse skeletal muscle. The whole lipid droplet proteins were subjected to 2D-LC−MS/MS analysis. The proteins listed in the table are part of proteins identified from skeletal muscle lipid droplets. √, The protein has been reported on lipid droplet.

Information). Immunolabeling of apo A-I showed that its location pattern was different from other LD proteins that typically surround LDs, forming a ring-shaped image. The majority of apo A-I molecules were dispersed in the ER with only a few apo A-I-reactive foci on a subset but not all of the droplets (Figure 5C and SI3, Supporting Information). Meanwhile, we also found the colocalization of apo A-I with LDs and ER (SI3, bold arrowhead pointed). Apo E also had the similar pattern by Western blot analysis. The partial colocalization of lipid droplets and apo E by immunofluorescence verifies the Western blot finding (SI2 and SI4, Supporting Information). Considering the close relationship between LDs and the ER, we assumed that apo A-I maybe situated on some specific regions of ER membrane to implicate in the formation of LDs as apo B does or to be lipidated at those

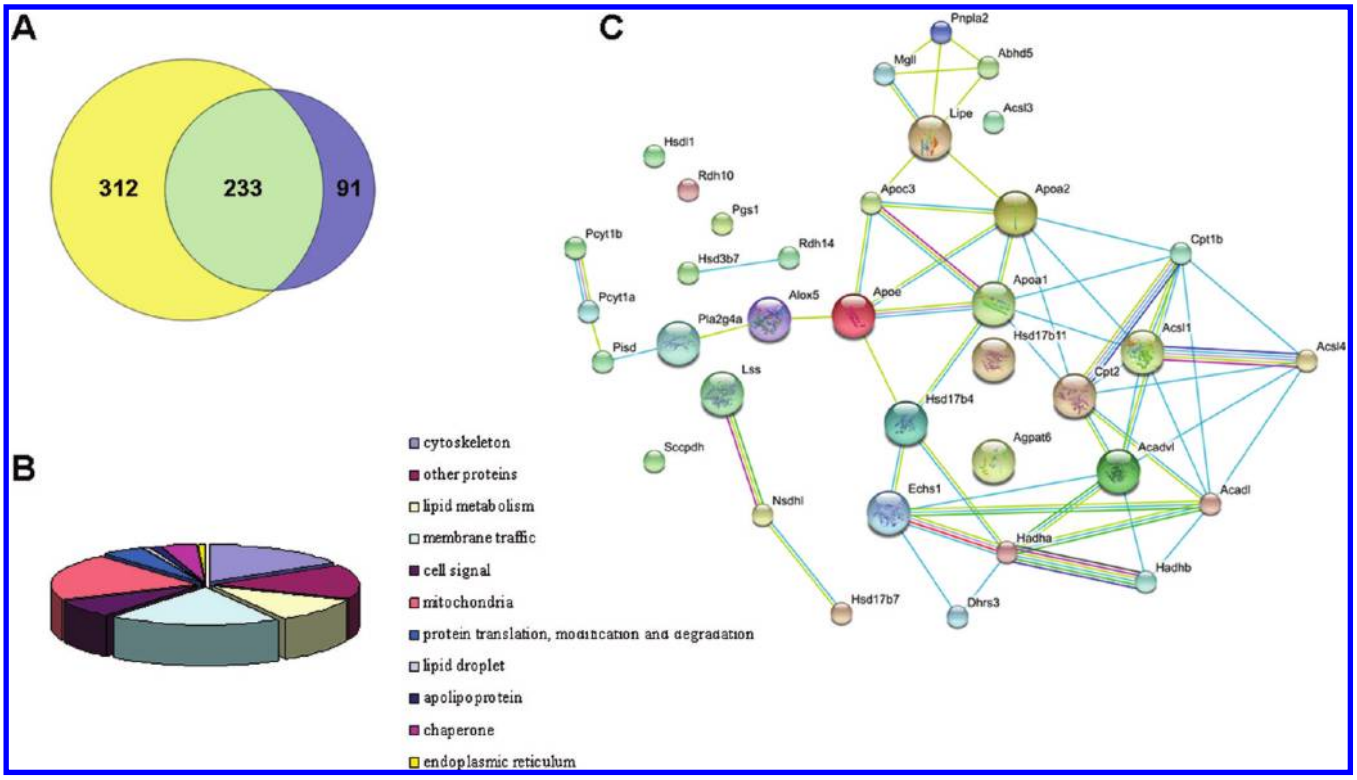

Figure 3. Properties of mouse skeletal muscle LD proteins. (A) Venn diagram shows the cross-correlation of identified LD proteins from mouse skeletal muscle (purple) and C2C12 myotube (yellow). Numbers inside the circle or overlaps separately represent proteins only belong or common to corresponding data sets. (B) All skeletal muscle LD proteins identified by 2D-LC−MS/MS were categorized by subcellular distributions and known functions based on literature or NCBI online sources. (C) Association network of identified metabolic proteins and apolipoproteins predicted by Web site program STRING against mouse database. Network edges represent predicted functional associations with different line colors standing for various types of evidence used for predicting: red, fusion evidence; green, neighborhood evidence; blue, co-occurrence evidence; purple, experimental evidence; yellow, text-mining evidence; black, co-expression evidence.

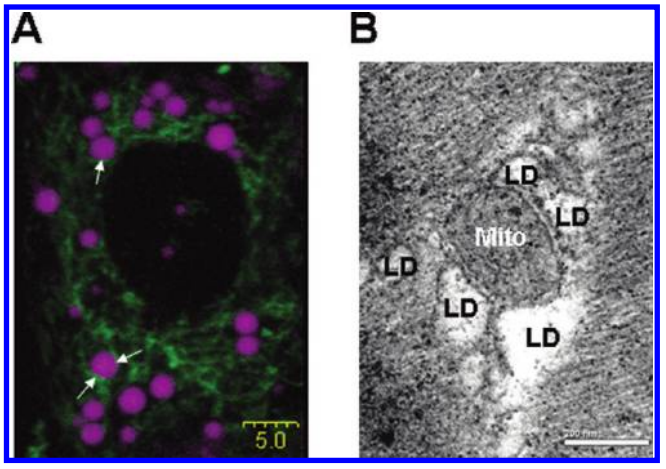

Figure 4. Interaction of LDs and mitochondria. (A) C2C12 cells pretreated with 200 μM oleate (12 h) were stained by MitoTracker Green FM (25 nM) and LipidTOX Deep Red (1:1000 diluted) for 30 min to stain mitochondria (green) and LDs (mauve), respectively. The white arrows indicate the interaction sites between these two organelles. Bar = 5 μm. (B) Mouse skeletal muscle was ultrathin sectioned and examined by TEM. LDs appeared close to or interacting with mitochondria. Bar = 200 nm.

positions.[5] Of course, the exact function of apo A-I on LDs remains further determined. Since we observed the apo A-I signal in C2C12 cultured with serum-free medium (Figure 5C), we further detected the endogenous expression by skeletal muscle. RT-PCR showed that human and mouse skeletal muscle as well as C2C12 could express apo A-I endogenously (Figure 5D−F). Notably, we also observed the endogenous expression of apo A-I in human heart (Figure 5D). However, the expression level of apo A-I in heart or skeletal muscle was significantly less than that in liver, which may be the possible reason why apo A-I was undetectable in other tissues except for liver and intestine in previous research.

DISCUSSION

The study presented here was set up to systematically identify the lipid droplet-associated proteins of skeletal muscle and C2C12 myotubes by applying 2D-LC−MS/MS analysis to the purified organelle. The identified proteins were categorized into several groups according to their functions and subcellular locations. Based on the proteomic, microscopic and immunoblotting results, mitochondria and apo A-I were found closely associating with LDs in skeletal muscle.

In fact, besides the well studied LD protein members including PAT family proteins, membrane traffic proteins and enzymes of lipid metabolism, our proteomic research also found 234 newly identified proteins on skeletal muscle LDs. Many of these proteins previously have been localized on other organelles such as ER or mitochondria rather than LDs (Table 1, Figure 3B),

dx.doi.org/10.1021/pr200553c |J. Proteome Res. 2011, 10, 4757–4768

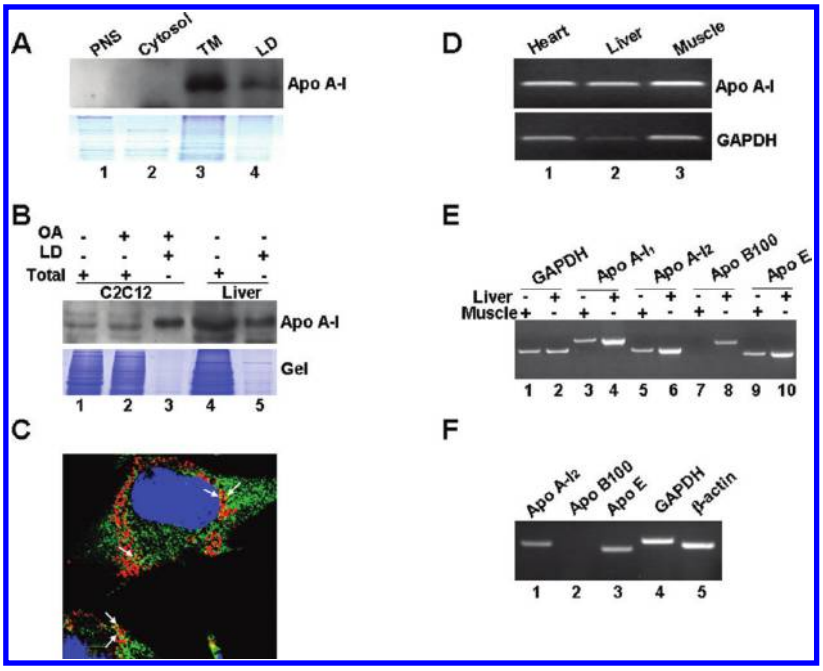

Figure 5. Localization and expression of apo A-I in mouse skeletal muscle and C2C12 myotube. (A and B) Apo A-I was determined on LDs of mouse skeletal muscle (A), liver and C2C12 myotube with or without oleate treatment (B) by immunoblotting. Colloidal Blue stained gel was utilized to present protein loading. (C) C2C12 cells were cultured with serum-free medium and pretreated with 200 μM oleate for 12 h, then incubated with rabbit antiapo A-I polyclonal antibody at room temperature for 1 h and FITC-conjugated secondary antibody for another 1 h to detect apo A-I (green). Nuclei were stained with Hoechst 33258 (blue) and LDs were stained with LipidTOX Deep Red (red). The white arrowheads indicate the sites where apo A-I bound to LDs. (D−F) RT-PCR was performed to detect endogenous apo A-I expression in human (D) and mouse skeletal muscle (E) as well as C2C12 myotube (F).

suggesting a potential relationship between LDs and other cellular compartments. Such relationships are feasible since presumptive functions of LDs, including energy homeostasis, membrane trafficking, lipid homeostasis and intracellular signaling, likely require intimate collaboration with other organelles. Previous studies including those from our laboratory have confirmed this conjecture and indicated that Rab18 and Rab5 were responsible for regulating the binding of LDs with ER or with endosomes,[22−24] we also found the interaction between LDs and mitochondria in *Saccharomyces cerevisiae* by using bimolecular fluorescence complementation assay.[43]

Among these LD-associated proteins, mitochondrial components occupied a large portion (65 molecules), and 57 of them were involved in TCA cycle (Table 1, Figure 3B). Since the amount of lipid droplet-bound mitochondria was relatively small in the isolated lipid droplets, it is possible that the relative abundant mitochondrial matrix proteins were first to be identified but some of the membrane proteins might be missed. Subsequent results of TEM, fluorescence microscopy and immunoblotting directly indicated the strong interaction of LDs and mitochondria in skeletal muscle (Figures 1A and 4). Indeed, the SNARE protein SNAP23 was found to participate in the formation of a LD−mitochondrion complex according to a recent study.[39] LDs in skeletal muscle fibers provide a fuel source for muscle action during periods of physical activity.[44] Mitochondria provide the primary source of energy during aerobic respiration and the close relationship between LDs and mitochondria likely permits more efficient deliver of fatty acids as a substrate for β-oxidation. In a previous study, an examination of highly trained atheletes' muscles revealed an increased number of small lipid droplets along with increased activity of lipid hydrolyase and fatty acid oxidase compared with nonatheletes, consistent with a greater capacity for energy mobilization.[44,45] Despite this beneficial association, in cases where lipid storage and energy utilization are unbalanced, the relationship between intramuscular LDs and mitochondria can lead to incomplete fatty acid oxidation, resulting in the development of insulin resistance.[46] Collectively, previous work and the current results illustrate that the interrelationship between mitochondria and LDs must be carefully regulated and further study of their functional and structural connections are likely to lead to a deeper understanding of how insulin insensitivity develops.

LDs and lipoprotein particles are two important structures involved in maintaining lipid homeostasis at the cellular and organismal levels.[47,48] They have similar composition and both originate from ER, but still can be distinguished by their size, function and location. Previous research found that two very low density lipoprotein (VLDL) apolipoproteins, apo B100 and apo A-V, were found associated with intracellular LDs and were important in regulated the neutral lipid levels of hepatocytes.[5,6] Furthermore, a novel apolipoprotein, apo O, was found associated with cardiomyocyte LDs, and may be involved in protecting the heart from lipoapoptosis in cases of obesity or diabetes mellitus by promoting lipid trafficking.[42] Here, using proteomics, immunoblotting and immunofluorenscence analyses, we found that apo A-I, the major component of HDL particles, was also present on LDs of skeletal muscle and C2C12. Additionally, other HDL-associated apolipoproteins including apo A-II, apo C-III and apo E were also identified in our mass spectrometry analysis (Table 1). Apo A-I is known to be expressed in the liver and intestine. Here, we reported RT-PCR results demonstrating that it is also expressed in skeletal muscle, although at a lower

level than in liver (Figure 5D−F). Therefore, it is possible that the LD-associated apo A-I is derived from the myocyte and is not from the uptake of external HDL, and our immunofluorescence result in C2C12 supported this presumption. Previous studies have found apo A-I expression in other cell types including pancreatic exocrine cells where it is secreted,[49] knee joint chondrocytes and retinal pigment epithelium.[50,51] Therefore, it is likely that apo A-I may have novel functions in addition to its accepted role on serum HDL. Naturally, more study concerning the exact functions of apo A-I in these novel contexts will be required.

CONCLUSION

In this study we identified 324 LD-associated proteins in skeletal muscle by mass spectrometry and further confirmed the close association of skeletal muscle LDs with mitochondria and apo A-I by electron microscopy, immunoblotting and immunofluorescence assays. These results offer new insights into the intricate metabolic functions in skeletal muscle and may promote new directions in future research concerning the etiology and treatment of type 2 diabetes.

ASSOCIATED CONTENT

Supporting Information

Supporting Information 1 (SI1)−Supporting Information 6 (SI7). This material is available free of charge via the Internet at http://pubs.acs.org.

AUTHOR INFORMATION

Corresponding Author

*Pingsheng Liu, Tel.: +86-10-64888517. Fax: +86-10-64888517. E-mail: pliu@sun5.ibp.ac.cn. Fuquan Yang, Tel: +86-10-64888581. Fax: +86-10-64888581. E-mail:fqyang@sun5.ibp.ac.cn.

Author Contributions

‡These authors contributed equally to this work.

ACKNOWLEDGMENT

We thank Dr. John K. Zehmer for his critical reading and useful suggestions. This work was supported by grants: the Ministry of Science and Technology of China (Grant No. 2009CB919000; Grant No. 2010CB833703), the National Natural Science Foundation of China (Grant No. 30871229 and Grant No. 30971431).

REFERENCES

(1) Murphy, D. J. The biogenesis and functions of lipid bodies in animals, plants and microorganisms. *Prog. Lipid Res.* **2001**, *40* (5), 325–438.

(2) Khandelia, H.; Duelund, L.; Pakkanen, K. I.; Ipsen, J. H. Triglyceride blisters in lipid bilayers: implications for lipid droplet biogenesis and the mobile lipid signal in cancer cell membranes. *PLoS One* **2010**, *5* (9), e12811.

(3) Murphy, D. J.; Vance, J. Mechanisms of lipid body formation. *Trends Biochem. Sci.* **1999**, *24* (3), 109–15.

(4) Zehmer, J. K.; Bartz, R.; Bisel, B.; Liu, P. S.; Seemann, J.; Anderson, R. G. W. Targeting sequences of UBXD8 and AAM-B reveal that the ER has a direct role in the emergence and regression of lipid droplets. *J. Cell Sci.* **2009**, *122* (20), 3694–702.

(5) Ohsaki, Y.; Cheng, J.; Suzuki, M.; Fujita, A.; Fujimoto, T. Lipid droplets are arrested in the ER membrane by tight binding of lipidated apolipoprotein B-100. *J. Cell Sci.* **2008**, *121* (Pt 14), 2415–22.

(6) Shu, X.; Chan, J.; Ryan, R. O.; Forte, T. M. Apolipoprotein A-V association with intracellular lipid droplets. *J. Lipid Res.* **2007**, *48* (7), 1445–50.

(7) Goldstein, J. L.; Dana, S. E.; Brown, M. S. Esterification of low density lipoprotein cholesterol in human fibroblasts and its absence in homozygous familial hypercholesterolemia. *Proc. Natl. Acad. Sci. U.S.A.* **1974**, *71* (11), 4288–92.

(8) Goldstein, J. L.; Brown, M. S. Binding and degradation of low density lipoproteins by cultured human fibroblasts. Comparison of cells from a normal subject and from a patient with homozygous familial hypercholesterolemia. *J. Biol. Chem.* **1974**, *249* (16), 5153–62.

(9) Farese, R. V.; Walther, T. C. Lipid Droplets Finally Get a Little R-E-S-P-E-C-T. *Cell* **2009**, *139* (5), 855–60.

(10) Wolins, N. E.; Brasaemle, D. L.; Bickel, P. E. A proposed model of fat packaging by exchangeable lipid droplet proteins. *Febs Lett* **2006**, *580* (23), 5484–91.

(11) Fujimoto, T.; Parton, R. G. Not Just Fat: The Structure and Function of the Lipid Droplet. *Csh Perspect. Biol* **2011**, *3* (3), a004838.

(12) Zimmermann, R.; Strauss, J. G.; Haemmerle, G.; Schoiswohl, G.; Birner-Gruenberger, R.; Riederer, M.; Lass, A.; Neuberger, G.; Eisenhaber, F.; Hermetter, A.; Zechner, R. Fat mobilization in adipose tissue is promoted by adipose triglyceride lipase. *Science* **2004**, *306* (5700), 1383–6.

(13) Ducharme, N. A.; Bickel, P. E. Minireview: Lipid droplets in lipogenesis and lipolysis. *Endocrinology* **2008**, *149* (3), 942–9.

(14) Harris, C. A.; Haas, J. T.; Streeper, R. S.; Stone, S. J.; Kumari, M.; Yang, K.; Han, X. L.; Brownell, N.; Gross, R. W.; Zechner, R.; Farese, R. V. DGAT enzymes are required for triacylglycerol synthesis and lipid droplets in adipocytes. *J. Lipid Res.* **2011**, *52* (4), 657–67.

(15) Goodman, J. M. Demonstrated and inferred metabolism associated with cytosolic lipid droplets. *J. Lipid Res.* **2009**, *50* (11), 2148–56.

(16) Zhang, S.; Du, Y.; Wang, Y.; Liu, P. Lipid Droplet —— A Cellular Organelle for Lipid Metabolism. *Acta Biophys. Sin.* **2010**, *26* (2), 97–105.

(17) Yu, W.; Bozza, P. T.; Tzizik, D. M.; Gray, J. P.; Cassara, J.; Dvorak, A. M.; Weller, P. F. Co-compartmentalization of MAP kinases and cytosolic phospholipase A2 at cytoplasmic arachidonate-rich lipid bodies. *Am. J. Pathol.* **1998**, *152* (3), 759–69.

(18) Yu, W. G.; Cassara, J.; Weller, P. F. Phosphatidylinositide 3-kinase localizes to cytoplasmic lipid bodies in human polymorphonuclear leukocytes and other myeloid-derived cells. *Blood* **2000**, *95* (3), 1078–85.

(19) Cermelli, S.; Guo, Y.; Gross, S. P.; Welte, M. A. The lipid-droplet proteome reveals that droplets are a protein-storage depot. *Curr. Biol.* **2006**, *16* (18), 1783–95.

(20) Zehmer, J. K.; Huang, Y. G.; Peng, G.; Pu, J.; Anderson, R. G. W.; Liu, P. S. A role for lipid droplets in inter-membrane lipid traffic. *Proteomics* **2009**, *9* (4), 914–21.

(21) Welte, M. A.; Cermelli, S.; Griner, J.; Viera, A.; Guo, Y.; Kim, D. H.; Gindhart, J. G.; Gross, S. P. Regulation of lipid-droplet transport by the perilipin homolog LSD2. *Curr. Biol.* **2005**, *15* (14), 1266–75.

(22) Ozeki, S.; Cheng, J. L.; Tauchi-Sato, K.; Hatano, N.; Taniguchi, H.; Fujimoto, T. Rab18 localizes to lipid droplets and induces their close apposition to the endoplasmic reticulum-derived membrane. *J. Cell Sci.* **2005**, *118* (12), 2601–11.

(23) Martin, S.; Driessen, K.; Nixon, S. J.; Zerial, M.; Parton, R. G. Regulated localization of Rab18 to lipid droplets: effects of lipolytic stimulation and inhibition of lipid droplet catabolism. *J. Biol. Chem.* **2005**, *280* (51), 42325–35.

(24) Liu, P.; Bartz, R.; Zehmer, J. K.; Ying, Y. S.; Zhu, M.; Serrero, G.; Anderson, R. G. Rab-regulated interaction of early endosomes with lipid droplets. *Biochim. Biophys. Acta* **2007**, *1773* (6), 784–93.

(25) Sturmey, R. G.; O'Toole, P. J.; Leese, H. J. Fluorescence resonance energy transfer analysis of mitochondrial: lipid association in the porcine oocyte. *Reproduction* **2006**, *132* (6), 829–37.

(26) Binns, D.; Januszewski, T.; Chen, Y.; Hill, J.; Markin, V. S.; Zhao, Y. M.; Gilpin, C.; Chapman, K. D.; Anderson, R. G. W.; Goodman, J. M. An intimate collaboration between peroxisomes and lipid bodies. *J. Cell Biol.* **2006**, *173* (5), 719–31.

(27) Machann, J.; Haring, H.; Schick, F.; Stumvoll, M. Intramyocellular lipids and insulin resistance. *Diabetes Obes. Metab.* **2004**, *6* (4), 239–48.

(28) Perseghin, G.; Scifo, P.; De Cobelli, F.; Pagliato, E.; Battezzati, A.; Arcelloni, C.; Vanzulli, A.; Testolin, G.; Pozza, G.; Del Maschio, A.; Luzi, L. Intramyocellular triglyceride content is a determinant of in vivo insulin resistance in humans: a 1H-13C nuclear magnetic resonance spectroscopy assessment in offspring of type 2 diabetic parents. *Diabetes* **1999**, *48* (8), 1600–6.

(29) Moro, C.; Bajpeyi, S.; Smith, S. R. Determinants of intramyocellular triglyceride turnover: implications for insulin sensitivity. *Am. J. Physiol. Endocrinol. Metab.* **2008**, *294* (2), E203–13.

(30) Kelley, D. E.; Goodpaster, B. H.; Storlien, L. Muscle triglyceride and insulin resistance. *Annu. Rev. Nutr.* **2002**, *22*, 325–46.

(31) Liu, P. S.; Ying, Y. S.; Zhao, Y. M.; Mundy, D. I.; Zhu, M. F.; Anderson, R. G. W. Chinese hamster ovary K2 cell lipid droplets appear to be metabolic organelles involved in membrane traffic. *J. Biol. Chem.* **2004**, *279* (5), 3787–92.

(32) Li, W. P.; Liu, P. S.; Pilcher, B. K.; Anderson, R. G. W. Cell-specific targeting of caveolin-1 to caveolae, secretory vesicles, cytoplasm or mitochondria. *J. Cell Sci.* **2001**, *114* (7), 1397–408.

(33) Shevchenko, A.; Wilm, M.; Vorm, O.; Mann, M. Mass spectrometric sequencing of proteins from silver stained polyacrylamide gels. *Anal. Chem.* **1996**, *68* (5), 850–58.

(34) Gasteiger, E.; Gattiker, A.; Hoogland, C.; Ivanyi, I.; Appel, R. D.; Bairoch, A. ExPASy: The proteomics server for in-depth protein knowledge and analysis. *Nucleic Acids Res.* **2003**, *31* (13), 3784–8.

(35) Kyte, J.; Doolittle, R. F. A simple method for displaying the hydropathic character of a protein. *J. Mol. Biol.* **1982**, *157* (1), 105–32.

(36) Ashburner, M.; Ball, C. A.; Blake, J. A.; Botstein, D.; Butler, H.; Cherry, J. M.; Davis, A. P.; Dolinski, K.; Dwight, S. S.; Eppig, J. T.; Harris, M. A.; Hill, D. P.; Issel-Tarver, L.; Kasarskis, A.; Lewis, S.; Matese, J. C.; Richardson, J. E.; Ringwald, M.; Rubin, G. M.; Sherlock, G.; Consortium, G. O. Gene Ontology: tool for the unification of biology. *Nat. Genet.* **2000**, *25* (1), 25–9.

(37) Jensen, L. J.; Kuhn, M.; Stark, M.; Chaffron, S.; Creevey, C.; Muller, J.; Doerks, T.; Julien, P.; Roth, A.; Simonovic, M.; Bork, P.; von Mering, C. STRING 8--a global view on proteins and their functional interactions in 630 organisms. *Nucleic Acids Res.* **2009**, *37* (Database issue), D412–6.

(38) Bartz, R.; Zehmer, J. K.; Zhu, M.; Chen, Y.; Serrero, G.; Zhao, Y.; Liu, P. Dynamic activity of lipid droplets: protein phosphorylation and GTP-mediated protein translocation. *J. Proteome Res.* **2007**, *6* (8), 3256–65.

(39) Jagerstrom, S.; Polesie, S.; Wickstrom, Y.; Johansson, B. R.; Schroder, H. D.; Hojlund, K.; Bostrom, P. Lipid droplets interact with mitochondria using SNAP23. *Cell Biol. Int.* **2009**, *33* (9), 934–40.

(40) Bostrom, P.; Andersson, L.; Rutberg, M.; Perman, J.; Lidberg, U.; Johansson, B. R.; Fernandez-Rodriguez, J.; Ericson, J.; Nilsson, T.; Boren, J.; Olofsson, S. O. SNARE proteins mediate fusion between cytosolic lipid droplets and are implicated in insulin sensitivity. *Nat. Cell Biol.* **2007**, *9* (11), 1286–93.

(41) Soni, K. G.; Mardones, G. A.; Sougrat, R.; Smirnova, E.; Jackson, C. L.; Bonifacino, J. S. Coatomer-dependent protein delivery to lipid droplets. *J. Cell Sci.* **2009**, *122* (11), 1834–41.

(42) Lamant, M.; Smih, F.; Harmancey, R.; Philip-Couderc, P.; Pathak, A.; Roncalli, J.; Galinier, M.; Collet, X.; Massabuau, P.; Senard, J. M.; Rouet, P. ApoO, a novel apolipoprotein, is an original glycoprotein up-regulated by diabetes in human heart. *J. Biol. Chem.* **2006**, *281* (47), 36289–302.

(43) Pu, J.; Ha, C. W.; Zhang, S.; Jung, J. P.; Huh, W. K.; Liu, P. Interactomic study on interaction between lipid droplets and mitochondria. *Protein Cell* **2011**, *2* (6), 487–96.

(44) He, J.; Goodpaster, B. H.; Kelley, D. E. Effects of weight loss and physical activity on muscle lipid content and droplet size. *Obes. Res.* **2004**, *12* (5), 761–9.

(45) Alsted, T. J.; Nybo, L.; Schweiger, M.; Fledelius, C.; Jacobsen, P.; Zimmermann, R.; Zechner, R.; Kiens, B. Adipose triglyceride lipase in human skeletal muscle is upregulated by exercise training. *Am. J. Physiol. Endocrinol. Metab.* **2009**, *296* (3), E445–53.

(46) Koves, T. R.; Ussher, J. R.; Noland, R. C.; Slentz, D.; Mosedale, M.; Ilkayeva, O.; Bain, J.; Stevens, R.; Dyck, J. R.; Newgard, C. B.; Lopaschuk, G. D.; Muoio, D. M. Mitochondrial overload and incomplete fatty acid oxidation contribute to skeletal muscle insulin resistance. *Cell Metab.* **2008**, *7* (1), 45–56.

(47) den Hartigh, L. J.; Connolly-Rohrbach, J. E.; Fore, S.; Huser, T. R.; Rutledge, J. C. Fatty Acids from Very Low-Density Lipoprotein Lipolysis Products Induce Lipid Droplet Accumulation in Human Monocytes. *J. Immunol.* **2010**, *184* (7), 3927–36.

(48) Jayaraman, S.; Gantz, D. L.; Gursky, O. Effects of phospholipase A(2) and its products on structural stability of human LDL: relevance to formation of LDL-derived lipid droplets. *J. Lipid Res.* **2011**, *52* (3), 549–57.

(49) Liu, P.; Li, W. P.; Machleidt, T.; Anderson, R. G. Identification of caveolin-1 in lipoprotein particles secreted by exocrine cells. *Nat. Cell Biol.* **1999**, *1* (6), 369–75.

(50) Simo, R.; Garcia-Ramirez, M.; Higuera, M.; Hernandez, C. Apolipoprotein A1 Is Overexpressed in the Retina of Diabetic Patients. *Am J Ophthalmol* **2009**, *147* (2), 319–325.

(51) Solomon, A.; Murphy, C. L.; Kestler, D.; Coriu, D.; Weiss, D. T.; Makovitzky, J.; Westermark, P. Amyloid contained in the knee joint meniscus is formed from apolipoprotein A-I. *Arthritis Rheum* **2006**, *54* (11), 3545–3550.